J Porous Mater (2016) 23:239–245
DOI 10.1007/s10934-015-0075-x

Synthesis, characterization and catalytic performance of ordered mesoporous Sn–Al catalysts

Zhiwei Zhou[1] · Pengcheng Yu[1] · Juan Qin[2] · Wenliang Wu[1] · Lin Xu[3] · Zhiqiang Gu[3] · Xiaoqin Liu[1]

Published online: 25 September 2015

Abstract A series of ordered mesoporous Sn–Al catalysts with high specific surface area, large pore volume and uniform pore size were successfully synthesized via facile one-pot evaporation induced self-assembly method. Different characterization techniques, such as XRD, N_2 adsorption–desorption, ICP, NH_3-TPD, TEM and UV-vis spectra were employed to investigate their physical chemical properties, and these catalysts were applied in the Baeyer–Villiger oxidation of cyclohexanone by molecular oxygen. The characteristic results showed that Sn–Al catalysts exhibited wormhole-like mesostructured and narrow pore-size distribution. The acidity of Sn–Al catalysts can be promoted by homogeneous incorporation of Sn species into the framework of Al_2O_3, which is beneficial to their catalytic performances in the Baeyer–Villiger oxidation of cyclohexanone by molecular oxygen. The Sn–Al catalyst when adding 7 % the weight percent of Sn in the catalyst shows higher yield of ε-caprolactone than other catalysts, and it exhibited excellent catalytic stability even after repeated reaction for five times.

Keywords Mesoporous materials · EISA method · Template synthesis · Baeyer–Villiger oxidation

✉ Zhiwei Zhou
zhiweizhou@njtech.edu.cn

[1] College of Chemistry and Chemical Engineering, Nanjing Tech University, Nanjing 210009, China

[2] Technology and Finance Service Center of Jiangsu Province, Nanjing 210042, China

[3] Jiangsu Yangnong Chemical Group Co., LTD., Yangzhou 225009, China

1 Introduction

Since the discovery of ordered mesoporous silicas in the 1990s [1, 2], ordered mesoporous materials (OMMs) have attracted continuous attentions owing to their superior textural properties, such as high specific area, regular framework and larger pore sizes with narrow distributions. For the applications in catalytic fields, OMMs, especially ordered non-siliceous mesoporous materials such as mesoporous metal oxides, heteroatom mesoporous zeolites and sulfates etc. [3–5], have been widely employed as either catalysts or supports [6–8] because its abundant ordered channels allow active components highly disperse in the mesostructure and strongly interact with OMMs.

Mesoporous metal oxides, as a kind of non-siliceous mesoporous materials, can be successfully templated with nanosizedor mesoporous carbon materials, silane-functionalized polymer, organic surfactants and cationic polymers etc [9–13]. A series of mesoporous metal oxides have been successfully synthesized through the sol–gel process [14–16] or by utilizing the nanocasting method [17, 18]. Among the above proposed processes, EISA pathway proposed by Grosso et al. [19] seems to be the most simple and facile method to get highly ordered and thermally stable mesoporous metal oxides or to get their supported materials because it can control the cross-bridging reaction of inorganic molecules from the dynamics. Ordered mesoporous alumina supported metal oxides have emerged as a new group of functional materials with enhanced catalytic performance [20–23]. In comparison to the wet impregnation of mesoporous alumina with metal oxide precursors, which often leads to its structure partially blockage and damage, mesoporous alumina supported metal oxides prepared by one-pot method is more suitable to achieve high-quality mesostructures that exhibit

strong metal-support interactions and retain homogeneous distribution of active sites [24].

In the various industrial catalytic processes, Lewis acid sites play a central role in the selective activation of functional groups in organic and biochemical transformations. Tetravalent tin (Sn^{4+}) incorporated into zeolite frameworks worked as highly active solid Lewis acid [25]. For example, Sn–Beta zeolite has been used in several important reactions, including Baeyer–Villiger oxidations [26], Meerwein–Ponndorf–Verley reductions [27], and epimerization of glucose [28, 29]. Additionally, mesoporous tin-containing silicates, such as Sn–MCM-41, have been used for acetalization of glycerol [30], conversion of trioses to lactates [31, 32], Mukaiyama-aldol reaction [33] and catalytic cellulose pyrolysis [34]. However, it is difficult for tetrahedrally Sn species to be incorporated into the carrier, who lacks active oxygen species such as SiO_2 and Al_2O_3 catalysts, because the precious metal species supported on carriers with reducible active oxygen species generally have a stronger interaction between metal species and carrier [35, 36]. Therefore, few works can be found on the mesoporous Sn–Al oxides besides the SnO_2/Al_2O_3 metal oxides prepared by a regular co-precipitation or decomposition method, which causes the separation of metal oxide phases.

The Baeyer–Villiger reaction is a type of reaction which offers the oxidation of ketones to esters or lactones. In general, B–V oxidation of cyclohexanone could be conducted by peroxyacids, organic peroxide and hydrogen peroxide as oxidants. However, oxidants mentioned above usually suffer from disadvantages regarding both the safety issues and intrinsic instability because they are explosive or corrosive and they should be handled with great caution. In addition, hydrogen peroxide is not stable and the oxidizing capacity is weak at low concentration, while it is dangerous and hard to obtain at high concentration [37]. In order to avoid these problems, molecular oxygen, as an environment friendly oxidant, is a better substitute because it is cheaper and safer. The catalytic performance of mesoporous metal oxides, especially composite oxides, was much higher than ordinary metal oxides in the B–V oxidation of cyclohexanone [38, 39]. In addition, the catalytic performance would be promoted by the incorporation of Sn species into the network of the carriers [26, 27, 40]. Therefore, the mesoporous Sn–Al catalysts would show high catalytic performance in the B–V oxidation of cyclohexanone.

In this paper, a facile one-pot EISA strategy was employed to synthesize a series of ordered mesoporous Sn–Al catalysts with different Sn species loadings. The characterization of XRD, N_2 adsorption–desorption, ICP, NH_3-TPD, UV-vis spectra and TEM were utilized to investigate their chemical physical properties. Furthermore, the catalytic performance of mesoporous Sn–Al catalysts was investigated in the Baeyer–Villiger oxidation of cyclohexanone by molecular oxygen.

2 Experimental

2.1 Preparation of catalysts

Mesoporous Sn–Al catalysts were synthesized according to the literature [41] using the F127 ($EO_{106}PO_{70}EO_{106}$,$EO_{1/4}$ ethylene oxide, $PO_{1/4}$ propylene oxide) as a structure-directing agent. In a typical synthesis process, 3.2 g of F127 was dissolved in 20 ml anhydrous ethanol solution containing 0.6 g of citric acid and 1.6 g of hydrochloric acid. Then, 3.26 g of alumina isopropoxide and a required amount of tin tetrachloride (0, 0.09, 0.11, 0.13, 0.15, 0.17 g) were simultaneously added to the above solution. After being vigorously stirred at 303 K for 24 h, the resultant mixture was transferred to a dish and underwent solvent evaporation at 318 K for 48 h and thermal treatment at 373 K for another 24 h. The final product was calcined at 673 K in air for 5 h to remove the template and named as Sn–Al-x, where x stands for the weight percent of Sn in the catalysts.

2.2 Catalyst characterization

X-ray powder diffraction patterns of the catalysts were obtained on a Bruker D8 instrument with Ni-filtered Cu Kα radiation ($\lambda = 0.154$ nm) and operated at 40 kV and 30 mA. The scanning rate was 0.05(°) s^{-1} in the 2θ range from 0.75° to 6.0° (small angle) and 10.0° to 80.0° (wide angle). Nitrogen adsorption–desorption isotherms of the catalysts were measured at 77 K using a Micromeritics Tristar 3000 system. The surface area was calculated by using the Brunauer–Emmett–Teller (BET) method in the partial pressure (P/P_0) range from 0.01 to 0.99. The mesopore size distribution was obtained from the adsorption branch of the isotherms by using the Barrett–Joyner–Halenda (BJH) adsorption model. The Sn/Al ratio of catalysts was analyzed by inductively coupled plasma (ICP, Optima 2000 DV, PerkinElmer, USA) after the sample had been dissolved in HF solution. Temperature-programmed desorption of ammonia was carried out in a quartz U-tube reactor, and 300 mg sample was used for each measurement. The sample was pretreated in the stream at 823 K for 60 min and then cooled down to 373 K. After that, the NH_3/He mixture was switched on for 30 min and then was swept by the stream for 40 min. The temperature was raise from 423 to 823 K at a rate 10 K min^{-1}. The consumption of NH_3 in the reactant stream was recorded by thermal conductivity detector (TCD). Transmission electron

microscopy (TEM) analysis was performed on a JEOL 2010 microscope at 200 kV. Catalysts were dispersed in ethanol by ultrasonic. Then, a carbon-coated Cu TEM grid was dipped in the catalyst suspension and dried under vacuum at 353 K before analysis. The Ultraviolet-visible diffuse reflectance spectra were measured on a Lambda 950 ultraviolet-visible spectrophotometer, and the wavelength was in the range from 200 to 800 nm.

2.3 Baeyer–Villiger oxidation of cyclohexanone

The Baeyer–Villiger oxidation of cyclohexanone was performed in a three-neck flat bottom flask, where one neck was equipped with a reflux condenser and oxygen (10 ml/min) as oxidant was continuously introduced through another neck. In a typical process, 0.14 g catalyst was added into 0.5 g cyclohexanone using acetonitrile as solvent and benzaldehyde as pro-oxygenic agent. The mixture was kept at 343 K for 5 h with continuous stirring. At the completion of the reaction, the flask was cooled down to room temperature and the reaction mixture was analyzed on a SP-6890 gas chromatograph equipped with a SE-30 column (0.25 μm × 50 m) and a flame ionization detector (FID). Dodecane was chosen as an internal standard to calculate cyclohexanone conversion and ε-caprolactone selectivity.

3 Results and discussion

3.1 Catalysts characterization

The powder XRD patterns of the Sn–Al-x catalysts are shown in Fig. 1. As can be seen in Fig. 1a, the small-angle XRD patterns of all the catalysts have two well-defined peaks, a strong diffraction peak at about 1.2° and one weak peak at around 2.2°, which could be indexed as the (100) and (110) reflections of *p*6mm two-dimensional hexagonal structure. It can be concluded that ordered structure of Al_2O_3 can be kept well after the incorporation of Sn species. However, the XRD patterns appear less resolved and the intensity of the diffraction peaks are significantly decreased with the Sn species loading increasing, which can be attributed to the blockage of Sn species inside the pores possibly. It can be seen from Fig. 1b that the mesoporous walls of all the catalysts are amorphous and no obvious diffraction peaks concerning isolated SnO_2 or other tin-related compounds, which indicated that the Sn species were highly dispersed.

The N_2 adsorption–desorption isotherms and corresponding pore size distribution curves of Sn–Al-x catalysts are shown in Fig. 2, and the detailed textural properties are listed in Table 1. From Fig. 2a, it can be clearly seen that all the catalysts exhibited a typical IV-type isotherms with a steeper capillary condensation step occurred at a relative pressure (P/P_0) ranging from 0.40 to 0.70, suggesting their mesoporous character [42]. From Fig. 2b, it can be clearly seen that the pore sizes of these catalysts were narrowly distributed around 3–5 nm owing to the existence of uniform mesoporous system. In addition, with the increasing of Sn species from 0 to 7 %, the capillary condensation steps shifted to higher relative pressure, which can be concluded that the pore size was expanded by the introduction of Sn species. When the Sn species loading increased to 9 %, the pore size distribution became broader owing to partial destruction of the ordered mesoporous structure by excess Sn species possibly, which is in good agreement with the results of aforementioned XRD patterns. As seen from Table 1, the surface area, pore size and pore volume increased when the Sn species loading was from 0 to 7 %. With further increasing from 7 to 9 % of Sn species loading, these data

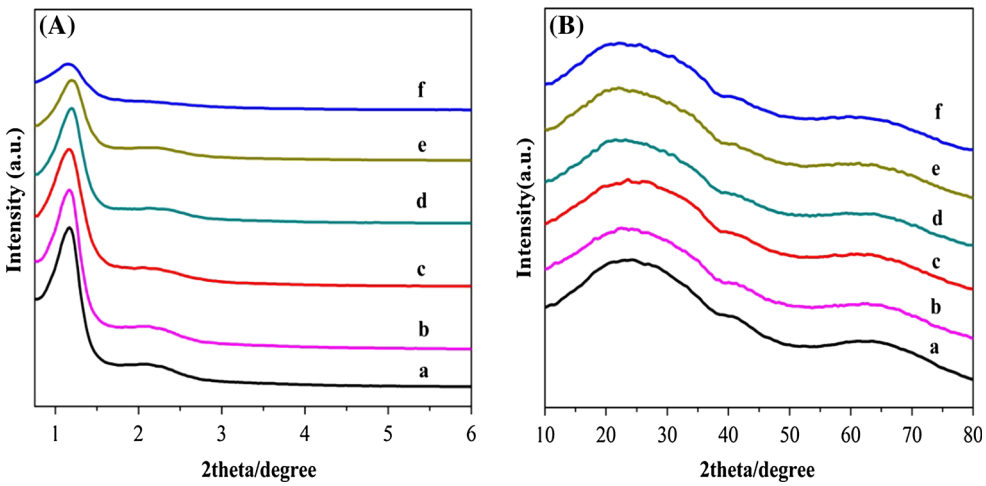

Fig. 1 Small-angle (**a**) and wide-angle (**b**) X-ray diffraction patterns of Sn–Al-x catalysts, *a* Sn–Al-0, *b* Sn–Al-5, *c* Sn–Al-6, *d* Sn–Al-7, *e* Sn–Al-8, *f* Sn–Al-9

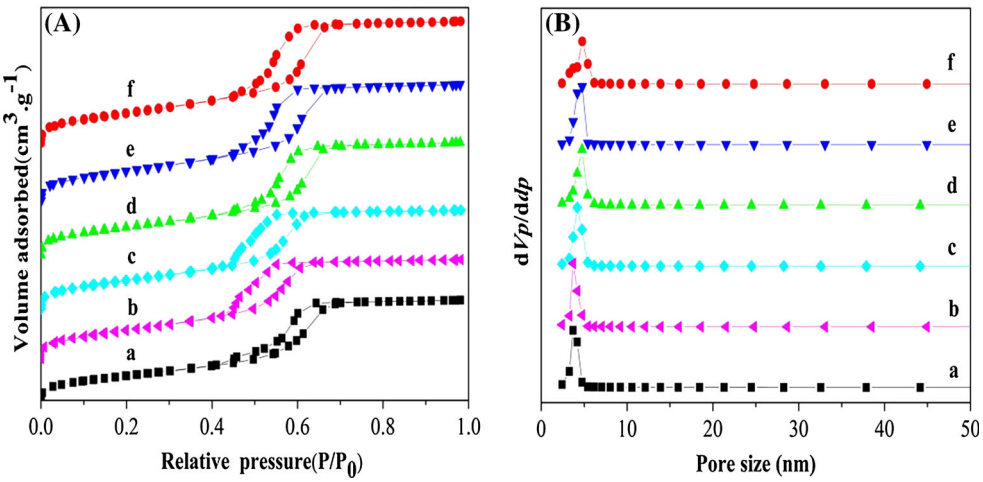

Fig. 2 N_2 adsorption–desorption isotherms (**a**) and pore size distribution curves (**b**) of Sn–Al-x catalysts, *a* Sn–Al-0, *b* Sn–Al-5, *c* Sn–Al-6, *d* Sn–Al-7, *e* Sn–Al-8, *f* Sn–Al-9

Table 1 Physical properties of different Sn–Al-x catalysts

Catalysts	Pore size (nm)[a]	S_{BET} (m^2 g^{-1})[b]	Pore volume (cm^3 g^{-1})[c]	Sn loading/(wt%)[d]
Sn–Al-0	3.7	280.9	0.37	0.0
Sn–Al-5	3.9	314.2	0.40	4.95
Sn–Al-6	4.2	322.4	0.42	6.02
Sn–Al-7	4.8	341.4	0.49	7.96
Sn–Al-8	4.8	335.5	0.47	8.01
Sn–Al-9	4.2	324.6	0.43	8.86

[a] BJH method

[b] BET specific areas

[c] $P/P_0 = 0.99$

[d] ICP-OES

decreased, which is might to the partial destruction of the mesoporous structure [5]. In addition, the actual loading of Sn species was almost the same as the feed ratio, suggesting that all the Sn species can be incorporated into the framework of Al_2O_3.

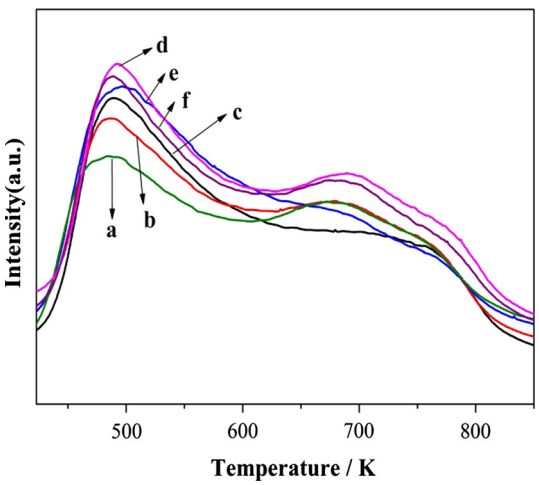

Fig. 3 NH_3-TPD curves for Sn–Al-x catalysts, *a* Sn–Al-0, *b* Sn–Al-5, *c* Sn–Al-6, *d* Sn–Al-7, *e* Sn–Al-8, *f* Sn–Al-9

The NH_3-TPD curves of different Sn–Al-x catalysts were obtained and the results are shown in Fig. 3. Two ammonia desorption peaks, one at low temperature and another at high temperature, were observed for all the six catalysts. Compared to the Sn–Al-0 catalyst, the total acid amount of another five Sn–Al catalysts prepared by EISA method increased, which indicated that the incorporation of Sn species into the framework of Al_2O_3 would be beneficial to its catalytic application. The Sn–Al-7 catalyst showed higher acid amount than another Sn–Al-x catalysts.

UV-vis spectroscopy was used to verify the coordination states of Sn species in the catalysts. It can be seen from Fig. 4 that no obvious bands can be observed for Sn–Al-0 catalysts. However, two bands, one centered at 210 nm and another centered at 265 nm, were observed for another five Sn–Al-x catalysts, which can be assigned to the formation of tetrahedrally [43, 44] and hexahedrally [45, 46] coordinated Sn species, respectively. Moreover, the intensities of these two bands had been promoted slightly with the Sn species loading increasing. No obvious absorption band centered at 400 nm can be observed, which indicated that no bulk SnO_2 particles were formed [47].

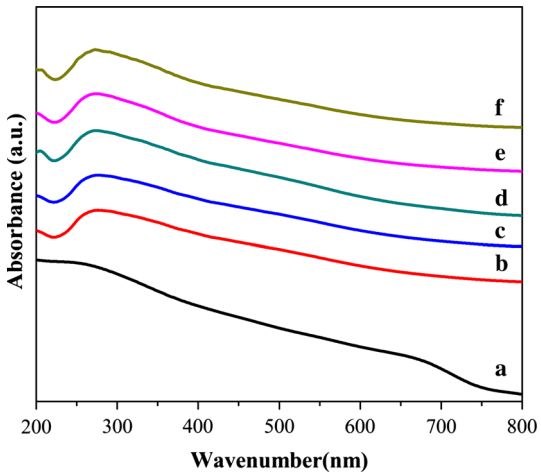

Fig. 4 UV-vis spectra of Sn–Al-x catalysts, *a* Sn–Al-0, *b* Sn–Al-5, *c* Sn–Al-6, *d* Sn–Al-7, *e* Sn–Al-8, *f* Sn–Al-9

To gain further insights into the morphological features, the TEM images of Sn–Al-x catalysts with different Sn species loadings were investigated, and the results are shown in Fig. 5. From Fig. 5, it can be clearly seen that all the Sn–Al-x catalysts exhibit similar wormhole-like pore structure, with no significant ordered pore arrangement. In addition, with the Sn species loadings increasing, the grain of the pores becomes more and more obscure owing to the blockage of Sn species inside the pores possibly, which is coincident with the results of the XRD patterns. This result demonstrated that after addition of Sn species, mesoporous Al_2O_3 frameworks were maintained. Combined with the nitrogen sorption analysis, the wormlike mesopores should have good interconnection in order to achieve the high surface area and pore volume.

3.2 Catalyst performance

The catalytic behaviors of different Sn–Al-x catalysts in the B–V oxidation of cyclohexanone by molecular oxygen are investigated and the results are listed in Table 2. From Table 2, 50.3 % conversion of cyclohexanone, 70.2 % selectivity of ε-caprolactone and 1.3 TON value can be obtained for Sn–Al-0 catalyst. With the Sn species loading increasing from 5 to 7 %, the conversion of cyclohexanone, the selectivity of ε-caprolactone and TON value increased, and then dropped at higher Sn species loading. The most active catalyst was Sn–Al-7, giving a cyclohexanone conversion of 90.8 %, ε-caprolactone selectivity of 91.7 % and 3.2 TON value, which may be owing to its highest acid amount, appropriate BET surface area, pore size and volume.

The catalytic stability for Sn–Al-7 catalyst was investigated, and the results are listed in Table 3. It can be seen that conversion of cyclohexanone, selectivity of ε-caprolactone and TON value decreased slightly, and they can reach to 84.5 %, 88.7 % and 2.9, respectively, after repeated reaction for 5 times, which suggested that the catalytic stability of Sn–Al-7 catalyst kept well.

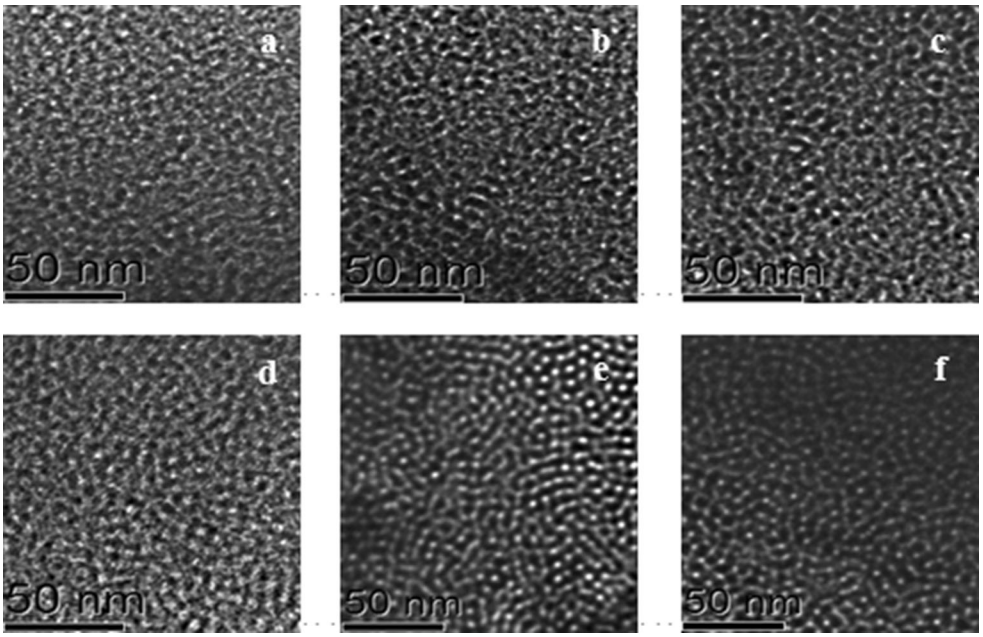

Fig. 5 TEM images of Sn–Al-x catalysts, **a** Sn–Al-0, **b** Sn–Al-5, **c** Sn–Al-6, **d** Sn–Al-7, **e** Sn–Al-8, **f** Sn–Al-9

Table 2 Catalytic performances of Sn–Al-x catalysts in the B–V oxidation of cyclohexanone

Catalysts	Cyclohexanone conversion/%	Caprolactone selectivity/%	TON[a]
Sn–Al-0	50.3	70.2	1.3
Sn–Al-5	76.3	80.2	2.3
Sn–Al-6	83.4	84.6	2.7
Sn–Al-7	90.8	91.7	3.2
Sn–Al-8	86.2	89.7	3.0
Sn–Al-9	79.4	83.2	2.6

Reaction conditions: w(catalyst)/w(cyclohexanone) = 0.28; w(acetonitrile)/w(cyclohexanone) = 30; w(benzaldehyde)/w(cyclohexanone) = 3; reaction time: 5 h; O_2: 10 ml/min; reaction temperature: 343 K

[a] Turnover number (TON): moles of product per mol of catalyst

Table 3 Catalytic stability for Sn–Al-7 catalyst in the B–V oxidation of cyclohexanone

Reaction number	Cyclohexanone conversion/%	Caprolactone selectivity/%	TON[a]
1	90.8	91.7	3.2
2	88.4	90.9	3.1
3	86.7	90.1	3.0
4	84.9	89.3	2.9
5	84.5	88.7	2.9

Reaction conditions: w(Sn–Al-7)/w(cyclohexanone) = 0.28; w(acetonitrile)/w(cyclohexanone) = 30; w(benzaldehyde)/w(cyclohexanone) = 3; reaction time: 5 h; O_2: 10 ml/min; reaction temperature: 343 K

[a] Turnover number (TON): moles of product per mol of catalyst

4 Conclusion

The mesoporous Sn–Al catalysts with high specific surface area (341.4 $m^2\ g^{-1}$), large pore volume (0.49 $cm^3\ g^{-1}$) and uniform pore size (4.8 nm) were synthesized by the evaporation induced self-assembly method in this paper. All the Sn species would be incorporated into the framework of Al_2O_3 and keep the wormhole-like structure. And the catalytic performance of Sn–Al catalysts in the B–V oxidation of cyclohexanone increased owing to its promoted acidity. A 90.8 % cyclohexanone conversion, 91.7 % selectivity of ε-caprolactone and 3.2 TON value could be obtained over the Sn–Al catalyst when adding 7 % the weight percent of Sn in the catalyst. In addition, the stability of this catalyst keeps well after repeated reaction for 5 times. Further studies to investigate mechanisms of the reaction are underway in our laboratory.

Acknowledgments This work was supported by Jiangsu Planned Projects for Postdoctoral Research Funds (1302121C); Open Project of Beijing Key Laboratory for Enze Biomass and Fine Chemicals; Project Funded by the Priority Academic Program Development of Jiangsu Higher Education Institutions.

References

1. C.T. Kresge, M.E. Leonowicz, W.J. Roth, J.C. Vartuli, J.S. Beck, Nature **359**, 710 (1992)
2. D.Y. Zhao, J.L. Feng, Q.S. Huo, N. Melosh, G.H. Fredrickson, B.F. Chmelka, G.D. Stucky, Science **279**, 548 (1998)
3. Y.X. Rao, M. Trudeau, D. Antonelli, J. Am. Chem. Soc. **128**, 13996 (2006)
4. Q. Yuan, A.X. Yin, C. Luo, L.D. Sun, Y.W. Zhang, W.T. Duan, H.C. Liu, C.H. Yan, J. Am. Chem. Soc. **130**, 3465 (2008)
5. L.L. Xu, H.L. Song, L.J. Chou, Int. J. Hydrog. Energy **38**, 7307 (2013)
6. D. Gu, F. Schuth, Chem. Soc. Rev. **43**, 313 (2014)
7. Q. Yuan, Q. Liu, W.G. Song, W. Feng, W.L. Pu, L.D. Sun, Y.W. Zhang, C.H. Yan, J. Am. Chem. Soc. **129**, 6698 (2007)
8. Z.C. Miao, H.L. Song, H.H. Zhao, L.L. Xu, L.Q. Chou, Catal. Sci. Technol. **4**, 838 (2014)
9. B. Lu, S. Chen, K. Kawamoto, Mater. Res. Bull. **47**, 3619 (2012)
10. L.L. Geng, X.Y. Zhang, W.X. Zhang, M.Q. Jia, G. Liu, Chem. Commun. **50**, 2965 (2014)
11. F. Jiao, P.G. Bruce, Angew. Chem. Int. Ed. **43**, 5958 (2004)
12. M.A. Carreon, V.V. Guliants, G.P.M. Olga, M.A. Bañares, Catal. Commun. **10**, 416 (2009)
13. C.A. Deshmane, J.B. Jasinski, M.A. Carreon, Microporous Mesoporous Mater. **130**, 97 (2010)
14. S. Li, H. Zhou, C.H. Jin, N.D. Feng, F. Liu, F. Deng, J.Q. Wang, W. Huang, L.P. Xiao, J. Fan, J. Phys. Chem. C **118**, 6283 (2014)
15. W. Wu, Z.J. Wan, W. Chen, H. Yang, D.K. Zhang, Adv. Powder Technol. **25**, 1220 (2014)
16. Y. Kamimura, M. Shimomura, A. Endo, J. Colloid Interface Sci. **436**, 52 (2014)
17. R.D. Zhang, P.X. Li, N. Liu, W.R. Yue, B.H. Chen, J. Mater. Chem. A **2**, 17329 (2014)
18. C.H. Yao, J. Wang, B. Li, Y.F. Shi, Mater. Lett. **110**, 65 (2013)
19. D. Grosso, F. Cagnol, G.J.A.A. de Soler-Illia, E.L. Crepaldi, H. Amenitsch, A. Brunet-Bruneau, A. Bourgeois, C. Sanchez, Adv. Funct. Mater. **14**, 309 (2004)
20. L. Kaluža, D. Gulková, O. Šolcová, N. Žilková, J. Čejka, Appl. Catal. A **351**, 93 (2008)

21. D. Dayananda, V.R. Sarva, S.V. Prasad, J. Arunachalam, P. Parameswaran, N.N. Ghosh, Appl. Surf. Sci. **329**, 1 (2015)
22. Y.Q. Gan, N. Tian, X.K. Tian, L.L. Ma, W.W. Wang, C. Yang, Z.X. Zhou, Y.X. Wang, J. Porous Mater. **22**, 147 (2015)
23. S. Badoga, R.V. Sharma, A.K. Dalai, J. Adjaye, Appl. Catal. A **489**, 86 (2015)
24. L.B. Sun, W.H. Tian, X.Q. Liu, J. Phys. Chem. C **113**, 19172 (2009)
25. Y. Román-Leshkov, M.E. Davis, ACS Catal. **1**, 1566 (2011)
26. A. Corma, L.T. Nemeth, M. Renz, S. Valencia, Nature **412**, 423 (2001)
27. A. Corma, M.E. Domine, L. Nemeth, S. Valencia, J. Am. Chem. Soc. **124**, 3194 (2002)
28. B.K. Chethana, S.H. Mushrif, J. Catal. **323**, 158 (2015)
29. N. Rajabbeigi, A.I. Torres, C.M. Lew, B. Elyassi, L.M. Ren, Z.P. Wang, H.J. Cho, W. Fan, P. Daoutidis, M. Tsapatsis, Chem. Eng. Sci. **116**, 235 (2014)
30. L. Li, T.I. Koranyi, B.F. Sels, P.P. Pescarmona, Green Chem. **14**, 1611 (2012)
31. L. Li, C. Stroobants, K.F. Lin, P.A. Jacobs, B.F. Sels, P.P. Pescarmona, Green Chem. **13**, 1175 (2011)
32. B. Murillo, A. Sánchez, V. Sebastián, C. Casado-Casado, O. de la Iglesia, M.P. López-Ram-de-Viu, C. Téllez, J. Coronas, J. Chem. Technol. Biotechnol. **89**, 1344 (2014)
33. M. Saito, H. Ikeda, Y. Horiuchi, M. Matsuoka, Res. Chem. Intermed. **40**, 87 (2014)
34. C. Torri, I.G. Lesci, D. Fabbri, J. Anal. Appl. Pyrolysis. **85**, 192 (2009)
35. T. Takeguchi, O. Takeoh, S. Aoyama, J. Ueda, R. Kikuchi, K. Eguchi, Appl. Catal. A **252**, 205 (2003)
36. X. Wang, R.J. Gorte, J.P. Wagner, J. Catal. **212**, 225 (2002)
37. Y.L. Ma, Z.Y. Liang, S.X. Feng, Y.D. Zhang, Appl. Organomet. Chem. **29**, 450 (2015)
38. W.H. Yao, H. Fang, E.C. Ou, J.Q. Wang, Z.Y. Yan, Catal. Commun. **7**, 387 (2006)
39. A.R. Ibrahim, L.H. Zhu, J. Xu, Y.Z. Hong, Y.Z. Su, H.T. Wang, B.H. Chen, J. Li, J. Supercrit. Fluids **92**, 190 (2014)
40. J.J. Jin, X.X. Ye, Y.S. Li, Y.Q. Wang, L. Li, J.L. Gu, W.R. Zhao, J.L. Shi, Dalton Trans. **43**, 8196 (2014)
41. D.H. Pan, M. Guo, M. He, S.W. Chen, X. Wang, F. Yu, R.F. Li, J. Mater. Res. **29**, 811 (2014)
42. S.Y. Chen, H.D. Tsai, W.T. Chuang, J.J. Lee, C.Y. Tang, C.Y. Lin, S. Cheng, J. Phys. Chem. C **113**, 15226 (2009)
43. R. van Grieken, C. Martos, M.S. Sánchez, D.P. Serrano, J.A. Melero, J. Iglesias, A.G. Cubero, Microporous Mesoporous Mater. **119**, 176 (2009)
44. P.P. Muthusamy, S. Kannan, L. Rafael, R. Anand, Green Chem. **15**, 2158 (2013)
45. R. Bermejo-Deval, R. Gounder, M.E. Davis, ACS Catal. **2**, 2705 (2012)
46. P. Li, G.Q. Liu, H.H. Wu, Y.M. Liu, J.G. Jiang, P. Wu, J. Phys. Chem. C **115**, 3663 (2011)
47. U.S. Taralkar, P. Kalita, R. Kumar, P.N. Joshi, Appl. Catal. A **358**, 88 (2009)